Available online at www.sciencedirect.com
SCIENCE DIRECT
Journal of Molecular Structure 795 (2006) 242–255
Journal of MOLECULAR STRUCTURE
www.elsevier.com/locate/molstruc

High resolution rotation–inversion spectroscopy on doubly deuterated ammonia, ND_2H, up to 2.6 THz

C.P. Endres [a,*], H.S.P. Müller [a,*], S. Brünken [a,1], D.G. Paveliev [b], T.F. Giesen [a], S. Schlemmer [a], F. Lewen [a]

[a] *I. Physikalisches Institut, Universität zu Köln, Zülpicher Str.77, 50937 Köln, Germany*
[b] *Department of Radiophysics, N. Novgorod State University, N. Novgorod, Russian Federation*

Received 7 February 2006; received in revised form 7 March 2006; accepted 7 March 2006
Available online 5 May 2006

The present work is dedicated to Gisbert Winnewisser on the occasion of his 70th birthday and in recognition of his many contributions to laboratory spectroscopy and astrophysics.

Abstract

Frequency multiplication of phase locked, high power backward wave oscillators (BWO) permitted to record high accuracy spectra of ND_2H up to frequencies of 2.6 THz. Novel superlattice (SL) devices were used as key-element to generate higher order harmonics for the first time in spectroscopic applications. In total, 240 measured ground state transitions of the pure rotation and inversion–rotation spectra of ND_2H were measured with accuracies of several kilohertz in the frequency region between 0.08 and 2.58 THz. Energy levels up to quantum numbers $J=18$ and $K_a=9$ have been accessed. A greatly extended experimental dataset was obtained with significantly improved accuracies. Two sets of molecular parameters have been determined from which predictions can be generated that can be regarded as a reliable basis for future astronomical high resolution observations throughout the microwave to terahertz regions. These predictions are available in the Cologne database for molecular spectroscopy (www.cdms.de).

Keywords: Terahertz spectroscopy; ND_2H; Ammonia; Superlattice semiconductor; Terahertz frequency multiplier

1. Introduction

Today, terahertz astronomy has evolved into a major field of astronomical and cosmological research. New ground based observatories, such as the Atacama pathfinder experiment (APEX), with which the first astronomical high resolution spectra at 1.5 THz have been recorded very recently [1], have opened the terahertz region for astronomical observations. The observable spectral region will be extended up to even higher frequencies by the upcoming Herschel space observatory. A multitude of spectral lines is expected in this frequency region stemming in part from well known molecules but also from hitherto unknown species thus demanding for high resolution spectroscopic data in the terahertz region in order to allow for unambiguous line assignments.

A significant part of spectral lines in the terahertz domain will be rotational transitions of light hydrides and their related deuterated isotopic species, including ammonia as an important example. The two partly deuterated ammonia species NH_2D and ND_2H exhibit comparatively rich spectra because of their asymmetry. The relevance of the deuterated species is underlined by the recent detection of doubly [2] and even triply deuterated ammonia [3,4] in interstellar space.

The ground vibrational state of ND_2H, which is the subject of the present investigations, has been studied previously by microwave and millimeter-wave techniques up to 515 GHz ($\approx 17\ cm^{-1}$) with estimated accuracies of 100 kHz. The most extensive set of measurements has been published by De Lucia and Helminger in 1975, who improved the quantitative description of the spectrum in their work [5]. Their calculation on the Coriolis interaction parameters underlined the necessity of the inclusion of such interaction terms to the Hamiltonian. Cohen and Pickett improved the model for both partly deuterated species and analyzed both inversion levels together [6]. They derived

* Corresponding authors. Tel.: +49 221 470 2757; fax: +49 221 470 5162.
E-mail addresses: endres@ph1.uni-koeln.de (C.P. Endres), hspm@ph1.uni-koeln.de (H.S.P. Müller).
[1] Present address: Division of Engineering and Applied Sciences, Harvard University, 29 Oxford Street, Cambridge, MA 02138, USA.

0022-2860/$ - see front matter © 2006 Elsevier B.V. All rights reserved.
doi:10.1016/j.molstruc.2006.03.035

important structural information about both partly deuterated isotopic species. A large dataset of around 700 far-infrared transitions of ND_2H up to 220 cm^{-1} with accuracies of $\sim$0.0003 cm^{-1} ($\approx$9 MHz) was supplemented by Fusina et al. in 1988 [7]. In addition, they reported several transition frequencies obtained in the microwave region. Their analysis yielded an improved parameter set, which already gave a fairly reliable basis for line predictions in the terahertz range.

Despite these investigations, the accuracies of calculated ND_2H transition frequencies were still not satisfactory to analyze future astronomical data in the terahertz domain, because they require line accuracies of better than 1 MHz. Therefore, we have extended the ND_2H dataset with the aim to provide reliable predictions for future astronomical observations and to test our new frequency multiplier setup.

Frequency multipliers have been successfully applied to terahertz spectrometers up to 1.6 THz [8] in Cologne for several years. Very recently, we have succeeded in applying the new efficient technique of harmonic generation with superlattice devices to record high resolution spectra up to 2.6 THz [9]. The use of these superlattice devices as key element for multiplication enabled us to extend the experimental dataset of rotation–inversion transitions of ND_2H by 240 lines with accuracies in the kilohertz range throughout. To our knowledge, these are the first molecular spectra ever recorded with this technique.

Ammonia and its isotopic species are not only very important astrochemical molecules, they are also very interesting from the spectroscopic point of view because of their prototypical large amplitude tunneling and the Coriolis interaction between the two tunneling states. Therefore, emphasis has also been put on recording transitions involving rotational levels heavily perturbed by Coriolis interaction.

The analysis presented in the current work includes the previously published data [5,7] and reproduces all reported experimental transitions within the estimated errors. The molecular parameters, in particular the Coriolis interaction terms, could be improved considerably. Based on this analysis highly accurate line predictions are provided in the catalog of the Cologne database for molecular spectroscopy (www.cdms.de) [10].

2. Experimental setup

All spectra were recorded with the Cologne spectrometers, which have been described in detail earlier [11,12]. The radiation is generated by phase locked backward wave oscillators (BWO). The use of harmonic generators provides a large extension of the operating range of this spectrometer. The novel technique of superlattice multipliers for the generation of higher harmonics was applied for the first time to spectroscopic studies [13,14]. Extensive investigations showed that radiation with multiplication factors of 3, 5, 7, 9, and 11 could be generated with considerable output power, which could be used to record spectra up to 2.6 THz.

A detailed description of this novel frequency multiplication technique is presented separately elsewhere [9]. At this point, a brief overview of the experimental setup shall be given. Only odd numbered harmonics are generated with sufficient intensities for spectroscopic applications because of the antisymmetry of the current–voltage characteristics of the superlattice device. Accuracies of $\Delta f/f = 10^{-11}$ can be achieved by phase locking the BWO to a rubidium reference frequency standard. A 2*f*-detection technique was employed to reduce base line effects and to improve the signal to noise ratio. A liquid helium cooled InSb hot electron bolometer (QMC) was used as detector.

The ND_2H sample was produced from a commercial ND_3 sample by H/D exchange with remaining H_2O inside the 3 m long absorption cell. The cell was conditioned with deuterated water to optimize the H/D ratio with respect to ND_2H. The total pressure was below 0.5 Pa for many transitions, in particular for stronger ones. It was raised for weaker lines up to about 5 Pa. All measurements have been carried out at room temperature. A short characterization of the set of lines and the number of recorded transitions associated with different spectrometer setups using either the fundamental or the multiplicated radiation is given in Table 1.

3. General properties of the spectrum

ND_2H is a very asymmetric rotor with the asymmetry parameter $\kappa = (2B - A - C)/(A - C)$ being -0.2284, indicating it to be a slightly prolate rotor. In contrast, NH_3 and ND_3 are oblate symmetric rotors, while NH_2D is, with $\kappa = -0.3117$, slightly less asymmetric than ND_2H. The spectrum of ND_2H exhibits the characteristics of an asymmetric top complicated by inversion and substantial rotation–inversion interaction. A comprehensive description of the spectrum, including the derivation of selection rules is given by De Lucia and Helminger [5]. Additional information, such as the orientation

Table 1
Overview of spectral lines measured in the course of the present investigation with different spectrometer setups. The frequency range (THz), accuracy (MHz) and maximum quantum numbers describe the set of lines measured with the given radiation source

Spectrometer	Frequency	Accuracy	J^{Max}	K_a^{Max}	K_c^{Max}	# Lines
BWO	0.078–0.891	0.01–0.3	18	9	11	105
BWO + SL	0.27–2.6	0.05–0.3	16	8	9	132
BWO + Tripler[a]	$\sim$2.4	0.2–0.4	7	5	4	3
Total	0.08–2.6		18	9	11	240

Blended lines are only counted once.
[a] A planar Schottky diode was available from the Jet Propulsion Laboratory for a few measurements [15].

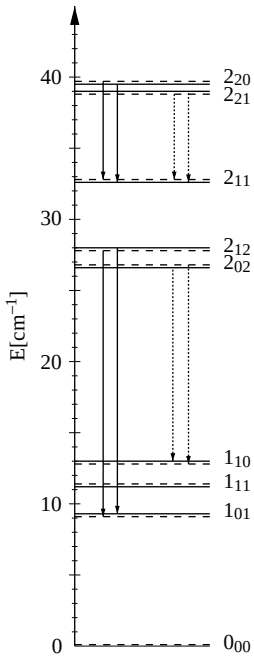

Fig. 1. Detail of the energy level diagram of the lowest rotational states of ND_2H. Each level is split into an upper ($v=1$) and a lower ($v=0$) inversion substate. b-Type transitions (solid arrows) occur within an inversion substate, while c-type transitions (dotted arrows) connect different substates. Para and ortho states are indicated by dashed and solid lines, respectively.

of the molecule and the dipole moment can be found in Ref. [6].

The tunneling effect causes a splitting of each rotational level into a doublet, whose components are designated as ortho and para states for K_a+K_c+v even and odd, respectively. The vibrational quantum number v labels the inversion substates with $v=0$ for the symmetric, lower state and $v=1$ for the antisymmetric, upper state. Distortion effects are quite large as is typical for light hydrides. Strong c-type transitions connect different inversion substates ($\Delta v=1$), whereas the weaker b-type transitions occur within these states ($\Delta v=0$) as depicted in Fig. 1. These selection rules are derived by considering the symmetry properties of the wave functions and the dipole matrix elements [5]. The hyperfine structure is dominated by quadrupole coupling due to the ^{14}N nucleus, which can be resolved partly in Doppler limited measurements for low-J transitions, whereas the coupling due to the two equivalent D nuclei is much weaker so that it could be neglected in this work.

Perturbations due to Coriolis interaction are found between closely spaced energy levels obeying the selection rules $\Delta J=0$, $\Delta K_a=0$, and $\Delta K_c=\pm 1$. As they are of equal symmetry, the upper asymmetry component of the lower inversion substate $v=0$ interacts with the lower asymmetry component of the upper inversion substate $v=1$. These Coriolis interactions are especially strong if the asymmetry splitting is comparable in size to the tunneling splitting. Three different cases of qualitatively different energy level separations are shown exemplarily in Fig. 2. In the case of $J=5$, $K_a=5$ and $K_c=0$, 1 the tunneling splitting is much larger than the asymmetry splitting, and levels of equal symmetry are well separated. For

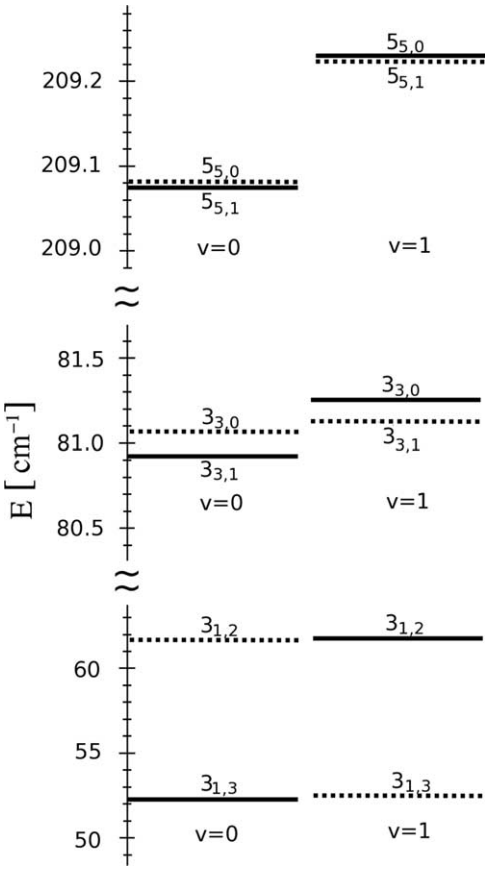

Fig. 2. Close up of the energy level diagram of ND_2H showing exemplarily the three different cases of tunneling splitting compared to the asymmetry splitting. Para and ortho states are indicated by dashed and solid lines, respectively. In the case of $J=5$, $K_a=5$ and $K_c=0$, 1 at the top, the tunneling splitting is much larger than the asymmetry splitting. For $J=3$, $K_a=3$ and $K_c=0$, 1 shown in the middle, the asymmetry splitting is increased and both splittings are comparable in size. Thus, the energy levels of both para states are close enough to distort each other significantly. In the third case at the bottom, $J=3$, $K_a=1$ and $K_c=2$, 3, the asymmetry splitting is even larger and hence the separation of levels of equal symmetry is too large to lead to a considerable interaction.

$J=3$, $K_a=3$ and $K_c=0$, 1, the asymmetry splitting is more pronounced, and both splittings are comparable in size. Thus the energy levels of both para states are close enough to repel each other significantly. In the third case, $J=3$, $K_a=1$ and $K_c=2$, 3 the asymmetry splitting is even larger, and hence the separation of levels of equal symmetry is again large.

Analysis of the ND_2H energy levels revealed that particularly strong interactions occur between levels with $J=2n+3$, $K_a=n+3$, $K_c=n+1$, $v=1$ and $J=2n+3$, $K_a=n+3$, $K_c=n$, $v=0$, for small values of n, e.g. the levels $J_{K_a,K_c}=3_{3,1}$, $v=1$ and $J_{K_a,K_c}=3_{3,0}$, $v=0$, shown in Fig. 2. A great number of strongly perturbed transitions have been recorded for energy levels described by $n=0$–4 in the course of the present investigations; furthermore, one transition has been measured which accesses the $J_{K_a,K_c}=13_{8,5}$, $v=0$ level.

4. Observed spectrum

Two hundred and forty transitions have been measured in total in the frequency range of 78 GHz–2.58 THz. Two

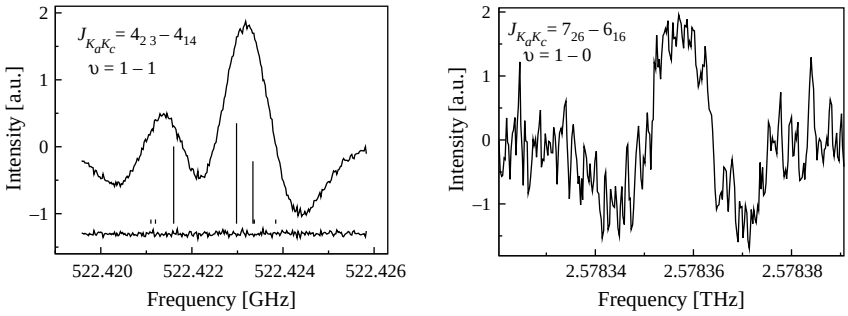

Fig. 3. Spectra of ND_2H at 522 GHz (left) and 2.58 THz (right) using the 5th and 11th harmonic of two different BWOs generated by a superlattice multiplier. The line profile of the lower transition shows hyperfine splitting which is displayed below as a stick diagram and which is well reproduced by the fit. The residuum of the calculation is shown at the bottom.

exemplary recordings are shown in Fig. 3. The rotational quantum number J reaches values up to 18 and the projections K_a and K_c values up to 9 and 11, respectively. One hundred and thirty five c-type transitions connecting the two inversion levels and 105 b-type transitions connecting levels within one inversion substate have been recorded. Of these, 16 lines have been remeasured to resolve the hyperfine splitting in part. Fifty-eight transition frequencies included in the dataset of Fusina et al. [7] have been determined with higher accuracies. Several of the newly recorded transitions have $\Delta K_a = 3$. They are comparatively strong because of the large asymmetry of the molecule, see Section 3.

Uncertainties for line positions were estimated individually for each transition and depend mainly on the signal-to-noise ratio, baseline effects, and on pressure induced line shifts. Pressure shifts of some lines have been determined representatively in order to estimate the influence of pressure and concentration effects on the line profiles and line center positions. It turned out that pressure shifts were in the range of 1–10 kHz/Pa which is comparable to shifts measured in the $v_2 = 1$ state of NH_3 [16].

Typical uncertainties for the lines measured in this work are 30–100 kHz. Even smaller uncertainties of 10 or 20 kHz were obtained for some lines with very good signal to noise ratio at lower frequencies or for the few transitions recorded in sub-Doppler mode while values up to 500 kHz were estimated for some noisy spectra in particular above 2 THz. Closed loops of transitions were used in many cases to check the error estimation. Transitions violating the loop criterion by more than five times the uncertainties were eliminated from the fit. The hyperfine splitting due to the ^{14}N nucleus was partly resolved for some transitions with low values of J. In these cases, the hyperfine structure is considered when fitting the line profiles and the center frequencies. Several transitions published in Ref. [5] have been remeasured, because deviations of up to 500 kHz were encountered in the fits. These deviations may originate from unresolved or partially resolved hyperfine splitting. This splitting reaches values of up to several megahertz for transitions with low values of J, as can be seen, for example, in the left part of Fig. 3.

5. Analysis and results

The analysis of the spectrum is based on an S-reduced Hamiltonian including terms up to the eighth power in the angular momentum operators. Fitting both inversion levels simultanously required interaction terms up to the eighth order in the angular momentum operators for an accurate description. Electric quadrupole hyperfine structure terms concerning ^{14}N have also been included. The prolate representation I^r has been chosen because slightly better results could be achieved initially compared to the oblate representation III^l. The reduced axis system (RAS) introduced by Pickett [17] has been used to derive the spectroscopic parameters in order to minimize the Coriolis effects. It was already applied to the partly deuterated ammonia isotopic species by Cohen and Pickett [6]. The Coriolis interaction term F_{bc}, in the following abbreviated as F, is an off-diagonal element of the inverse moments of inertia tensor. Thus, the rotational part and the interaction part of the Hamiltonian can be written as

$$\begin{aligned} H_{vv} &= E_v + A_v J_a^2 + B_v J_b^2 + C_v J_c^2 - D_K J_a^4 - D_{JK} J^2 J_a^2 - D_J J^4 \\ &+ d_1 J^2 (J_+^2 + J_-^2) + d_2 (J_+^4 + J_-^4) + H_K J_a^6 + H_{KJ} J^2 J_a^4 + H_{JK} J^4 J_a^2 \\ &+ H_J J^6 + h_1 J^4 (J_+^2 + J_-^2) + h_2 J^2 (J_+^4 + J_-^4) + h_3 (J_+^6 + J_-^6) \\ &+ L_K J_a^8 + L_{KKJ} J^2 J_a^6 + L_{JK} J^4 J_a^4 + L_{JJK} J^6 J_a^2 + L_J J^8 \\ &+ l_1 J^6 (J_+^2 + J_-^2) + l_2 J^4 (J_+^4 + J_-^4) + l_3 J^2 (J_+^6 + J_-^6) + l_4 (J_+^8 + J_-^8) + \ldots \end{aligned} \tag{1}$$

$$\begin{aligned} H_{01} = \{\{J_b, J_c\}, & F + F_J J^2 + F_K J_a^2 + F_{JJ} J^4 + F_{JK} J^2 J_a^2 \\ & + F_{KK} J_a^4 + F_{KKK} J_a^6 + F_{JKK} J^2 J_a^4 + F_{JJK} J^4 J_a^2 \\ & + F_{JJJ} J^6 + \ldots\}/2 \end{aligned} \tag{2}$$

E_v denotes the energy level of the inversion state. The subscripts v have been dropped for the distortion terms for breavity. The raising and descending operators are defined by $J_\pm = J_b \pm i J_c$. Finally, $\{,\}$ denotes the anticommutator. It is worthwhile mentioning that the anticommutator is redundant for terms not containing a power of J_a; it has been kept for breavity and clarity. Terms involving $(J_+^4 - J_-^4)/2i$, which can be viewed as asymmetry distortion terms of F and which

Table 2
Overview of the datasets used in the ND_2H-fit, including frequency range, maximum quantum numbers, weighted standard deviation RMS for each dataset with respect to fit 1/fit 2, and number of lines with blended lines only counted once

Reference	Frequency range	Accuracy	J^{Max}	K_a^{Max}	K_c^{Max}	RMS	# Lines
Refs. [5–7,20]	5–515 GHz	0.1 MHz	20	7	20	0.93/0.86	85
This work	0.08–2.6 THz	0.01–0.4 MHz	18	9	11	0.99/1.12	240
Fusina et al. [7]	17–220 cm^{-1}	$\geq$0.0003 cm^{-1} [a]	18	14	16	0.85/0.83	601
Global dataset			20	14	20	0.89/0.91	923

[a] $\approx$9 MHz; see Section 5.

connect levels with $\Delta K_a = 2$, were tested in the fits. Generally, they contributed little to the reduction of the weighted standard deviation of the fit. Moreover, they were strongly correlated with other terms such as d_1 or F_J. Therefore, these terms were omitted from the final fits.

The hyperfine part H_{vv}^{hfs} of the Hamiltonian is added to H_{vv} (Eq. (1)) and considered the ^{14}N nuclear electric quadrupole coupling only. It is described by the usual spectroscopic parameters χ_{bb} and χ_{cc}. Effects of the ^{14}N nuclear magnetic spin-rotation coupling and hyperfine terms due to the one H and two equivalent D nuclei were negligible.

Pickett's programs SPFIT and SPCAT [18] were employed to fit the experimental data including the large datasets of Fusina et al. [7] and De Lucia and Helminger [5] and to make predictions. Table 2 shows the datasets of transitions used in the final fits. No uncertainties were given for the transitions recorded in the microwave to millimeter-wave regions [5,7]. A value of 100 kHz appeared to be appropriate even though some lines showed much larger residuals in the previous fits [5,7]. Several trial fits indicated that the transition frequencies obtained by far-infrared Fourier transform spectroscopy [7] were reproduced to about 0.0003 cm^{-1} ($\approx$9 MHz), quite close to the estimated 0.00025 cm^{-1}. However, at lower frequencies larger residuals were encountered both in the fit and in closed loop calculations. Uncertainties of 0.0005 and 0.0004 cm^{-1} were adopted for the transition frequencies below 35 and from 35 to 45 cm^{-1}, respectively, 0.0003 cm^{-1} was used as uncertainty for the majority of the lines.

The Hamiltonian was reorganized in a way that the mean value $X = (X_0 + X_1)/2$ and the difference $\Delta X = (X_0 - X_1)/2$ of each parameter regarding both components $v = 0$ and 1 were included in the fit. Initial fit results were obtained by starting with a small set of parameters and a set of transitions limited to low values of J, the fit was extended step by step to higher J.

This approach, however, did not yield satisfactory results after the final round of measurements in which emphasis was put on highly perturbed transitions. Therefore, all spectroscopic parameters of a given order were included in the fit until the weighted standard deviation of the fit did not decrease anymore. Distortion and interaction parameters of eighth order were necessary in the fit to reproduce transitions with high-J values. A small number of transitions for which the experimental frequencies deviated from the calculated ones by more than 3.5 times their uncertainties were eliminated from the fit at this stage. On the other hand, several transitions poorly reproduced or eliminated from the final fit of Fusina et al. [7] were retained in the present fit. The final global dataset includes 923 different transition frequencies of which 240 have been measured in the course of the present investigation; overlapping hyperfine or asymmetry components have been counted only once.

Sixty-one parameters have been employed in this intermediate fit, which had a value of $\sim$0.85 as the weighted standard deviation of the fit. However, several parameters were correlated and could not be determined with significance. Therefore, their number was reduced by eliminating those, which contributed only marginally to the reduction of the weighted standard deviation of the fit. Two approaches were followed because the choice of spectroscopic parameters is generally not unique for such an extensive dataset of such a complex spectrum. In the first approach, distortion terms from H_{vv} were omitted while in the second one particularly terms from H_{01} were taken out of the fit. The elimination of nine and eight terms in fits 1 and 2, respectively, increased the weighted standard deviation of the fit from about 0.85 to about 0.90, indicating that overall the data still have been reproduced within the experimental uncertainties.

Table 3 summarizes the transition frequencies determined in the course of the present investigation, assignments, uncertainties and the residuals between observed and calculated frequencies with respect to fits 1 and 2. The complete line list with residuals from both fits is available as supplementary data and will also be available in the CDMS [10]. The spectroscopic parameters from fits 1 and 2 are presented in Table 4.

The dipole moment of ND_2H, required for line intensity predictions, is the averaged value of the dipole moments of NH_2D and ND_3. Using the experimental values $\mu = 1.495$ D for ND_3 [19] and $\mu = 1.477$ D for NH_2D [6], $\mu = 1.486$ D was interpolated for ND_2H.

The direction of the dipole moment is assumed to be parallel to the c_{NH_3}-axis of the NH_3 reference system. As the reduced axis system is used in the analysis, the components μ_b and μ_c of the dipole moments were derived by projecting the dipole moment onto the reduced axis system, using $\theta_R = -8.12°$ as given in Ref. [6], the angle between c-axis of the reduced axis system and the c_{NH_3}-axis. A sketch of the ND_2H molecule is displayed in Fig. 4, which also includes the orientation of the reduced axis system, together with the inertial axis system in the rigid rotor model and the NH_3 reference system, in which c_{NH_3} is perpendicular to the plane of the hydrogen atoms. As can be seen in Fig. 4, the c_r-axis of the reduced axis system is almost perpendicular to the plane of the three light atoms, whereas the b_r-axis directs towards the hydrogen. Thus, the

Table 3
Transition frequencies of doubly deuterated ammonia, ND_2H, observed in the course of the present investigation, their frequencies (MHz), uncertainties Unc. (kHz), residuals O–C 1 and O–C 2 between observed frequencies and those calculated from fit 1 and 2, respectively

J'', K_a'', K_c''–J', K_a', K_c'	v''–v'	F''–F'	Freq.	Unc.	O–C 1	O–C 2	IW
4, 2, 3–4, 1, 3	1–0	3–3	79,302.637	10	2	7	0.3646
4, 2, 3–4, 1, 3	1–0	3–4	79,302.637	10	2	7	0.0243
4, 2, 3–4, 1, 3	1–0	5–4	79,302.637	10	2	7	0.0244
4, 2, 3–4, 1, 3	1–0	5–5	79,302.637	10	2	7	0.5867
4, 2, 3–4, 1, 3	1–0	4–3	79,302.924	10	−2	3	0.0486
4, 2, 3–4, 1, 3	1–0	4–4	79,302.924	10	−2	3	0.9025
4, 2, 3–4, 1, 3	1–0	4–5	79,302.924	10	−2	3	0.0489
9, 4, 6–9, 3, 6	0–1		90,438.630	50	−18	−60	
14, 6, 9–14, 5, 9	0–1		93,121.009	50	62	101	
9, 4, 6–9, 3, 6	1–0		98,351.137	50	9	29	
14, 6, 9–14, 5, 9	1–0		98,577.772	50	24	109	
1, 1, 0–1, 0, 1	1–1	1–1	110,811.109	20	9	12	
1, 1, 0–1, 0, 1	1–1	1–2	110,811.711	20	−3	1	
1, 1, 0–1, 0, 1	1–1	2–1	110,812.271	20	17	21	
1, 1, 0–1, 0, 1	1–1	2–2	110,812.864	20	−4	1	
1, 1, 0–1, 0, 1	1–1	0–1	110,813.983	20	−2	3	
1, 1, 0–1, 0, 1	0–0	1–1	110,894.934	30	20	23	
1, 1, 0–1, 0, 1	0–0	1–2	110,895.541	30	12	17	
1, 1, 0–1, 0, 1	0–0	2–1	110,896.107	30	42	46	
1, 1, 0–1, 0, 1	0–0	2–2	110,896.660	30	−20	−14	
1, 1, 0–1, 0, 1	0–0	0–1	110,897.783	30	−9	−03	
6, 3, 4–6, 2, 4	0–1		118,504.182	50	−26	−41	
2, 1, 1–2, 0, 2	1–1		177,819.325	50	68	91	
2, 1, 1–2, 0, 2	0–0		177,921.203	50	83	93	
18, 8, 11–18, 7, 11	0–1		183,472.329	100	31	−58	
18, 8, 11–18, 7, 11	1–0		186,878.391	200	456	293	
15, 7, 9–15, 6, 9	0–1		248,927.534	50	−66	−3	
10, 5, 6–10, 4, 6	1–0		249,449.989	100	−48	−59	
10, 5, 6–10, 4, 6	1–0		249,450.038	50	1	−10	
15, 7, 9–15, 6, 9	1–0		253,639.645	50	−36	22	
4, 2, 2–4, 1, 3	1–1	4–4	268,026.502	30	−4	−1	0.9025
4, 2, 2–4, 1, 3	1–1	4–5	268,026.502	30	−4	−1	0.0489
4, 2, 2–4, 1, 3	1–1	4–3	268,026.502	30	−4	−1	0.0486
4, 2, 2–4, 1, 3	1–1	3–4	268,027.313	30	−38	−34	0.0243
4, 2, 2–4, 1, 3	1–1	3–3	268,027.313	30	−38	−34	0.3646
4, 2, 2–4, 1, 3	1–1	5–5	268,027.313	30	−38	−34	0.5867
4, 2, 2–4, 1, 3	1–1	5–4	268,027.313	30	−38	−34	0.0244
3, 1, 2–3, 0, 3	1–1	2–3	296,475.318	50	−24	20	0.0794
3, 1, 2–3, 0, 3	1–1	3–3	296,475.318	50	−24	20	0.8403
3, 1, 2–3, 0, 3	1–1	4–3	296,475.318	50	−24	20	0.0803
3, 1, 2–3, 0, 3	1–1	2–2	296,477.207	50	15	61	0.3175
3, 1, 2–3, 0, 3	1–1	3–2	296,477.207	50	15	61	0.0397
3, 1, 2–3, 0, 3	1–1	3–4	296,477.207	50	15	61	0.0402
3, 1, 2–3, 0, 3	1–1	4–4	296,477.207	50	15	61	0.6027
3, 1, 2–3, 0, 3	0–0	2–3	296,614.242	20	−33	−22	0.0794
3, 1, 2–3, 0, 3	0–0	3–3	296,614.242	20	−33	−22	0.8403

(*continued on next page*)

Table 3 (*continued*)

J'', K_a'', K_c''–J', K_a', K_c'	v''–v'	F''–F'	Freq.	Unc.	O–C 1	O–C 2	IW
3, 1, 2–3, 0, 3	0–0	4–3	296,614.242	20	−33	−22	0.0803
3, 1, 2–3, 0, 3	0–0	2–2	296,616.132	20	7	19	0.3175
3, 1, 2–3, 0, 3	0–0	3–4	296,616.132	20	7	19	0.0402
3, 1, 2–3, 0, 3	0–0	3–2	296,616.132	20	7	19	0.0397
3, 1, 2–3, 0, 3	0–0	4–4	296,616.132	20	7	19	0.6026
12, 6, 7–12, 5, 7	0–1		318,728.295	50	52	−1	
1, 1, 1–0, 0, 0	1–1	0–1	335,445.431	10	8	4	
1, 1, 1–0, 0, 0	1–1	2–1	335,446.240	10	13	7	
1, 1, 1–0, 0, 0	1–1	1–1	335,446.760	10	−4	−10	
1, 1, 1–0, 0, 0	0–0	0–1	335,512.892	10	−2	0	
1, 1, 1–0, 0, 0	0–0	2–1	335,513.715	10	12	13	
1, 1, 1–0, 0, 0	0–0	1–1	335,514.248	10	5	5	
2, 2, 0–2, 1, 2	0–1	2–2	346,351.162	50	−3	28	
2, 2, 0–2, 1, 2	0–1	1–2	346,353.232	50	−112	−78	0.0971
2, 2, 0–2, 1, 2	0–1	2–1	346,353.232	50	−112	−78	0.0971
2, 2, 0–2, 1, 2	0–1	3–3	346,353.232	50	−112	−78	0.8058
2, 2, 0–2, 1, 2	0–1	1–1	346,354.642	50	−66	−29	
6, 3, 3–6, 2, 4	1–1		351,982.597	50	20	−13	
2, 2, 0–2, 1, 2	1–0	2–2	356,227.422	20	2	−1	
2, 2, 0–2, 1, 2	1–0	2–3	356,228.565	20	4	2	0.5000
2, 2, 0–2, 1, 2	1–0	3–2	356,228.565	20	4	2	0.5000
2, 2, 0–2, 1, 2	1–0	1–2	356,229.611	20	7	7	0.0971
2, 2, 0–2, 1, 2	1–0	2–1	356,229.611	20	7	7	0.0971
2, 2, 0–2, 1, 2	1–0	3–3	356,229.611	20	7	7	0.8057
2, 2, 0–2, 1, 2	1–0	1–1	356,230.980	20	9	11	
2, 0, 2–1, 1, 0	0–1	1–0	410,487.790	40	−40	−41	
2, 0, 2–1, 1, 0	0–1	3–2	410,490.136	20	−6	−5	
2, 0, 2–1, 1, 0	0–1	2–1	410,492.338	20	−4	0	
14, 7, 8–14, 6, 8	1–0		410,887.220	50	5	18	
3, 2, 2–3, 1, 3	0–0	2–3	414,788.768	50	20	−2	0.0794
3, 2, 2–3, 1, 3	0–0	3–3	414,788.768	50	−20	−2	0.8403
3, 2, 2–3, 1, 3	0–0	4–3	414,788.768	50	−20	−2	0.0804
3, 2, 2–3, 1, 3	0–0	2–2	414,790.567	50	29	50	0.3175
3, 2, 2–3, 1, 3	0–0	3–2	414,790.567	50	29	50	0.0397
3, 2, 2–3, 1, 3	0–0	3–4	414,790.567	50	29	50	0.0402
3, 2, 2–3, 1, 3	0–0	4–4	414,790.567	50	29	50	0.6027
6, 4, 2–6, 3, 3	1–1		440,102.126	50	−19	−28	
3, 3, 0–3, 2, 2	0–1		442,398.115	50	38	42	
3, 3, 1–3, 2, 2	0–0		443,297.355	50	5	−10	
3, 3, 1–3, 2, 2	1–1		444,316.915	50	−36	−33	
7, 3, 4–7, 2, 5	1–1		461,050.791	50	−30	−77	
7, 2, 5–6, 5, 1	1–0		486,572.692	50	1	56	
5, 4, 2–5, 3, 2	0–1		487,342.420	50	1	−10	
5, 4, 2–5, 3, 2	1–0		495,682.955	50	−13	−3	
3, 2, 1–3, 1, 3	1–0	2–3	500,437.761	50	−6	15	0.0794
3, 2, 1–3, 1, 3	1–0	3–3	500,437.761	50	−6	15	0.8403
3, 2, 1–3, 1, 3	1–0	4–3	500,437.761	50	−6	15	0.0803
3, 2, 1–3, 1, 3	1–0	2–2	500,440.130	50	−45	−22	0.3175

3, 2, 1–3, 1, 3	1–0	3–4	500,440.130	50	−45	−22	0.0402
3, 2, 1–3, 1, 3	1–0	3–2	500,440.130	50	−45	−22	0.0397
3, 2, 1–3, 1, 3	1–0	4–4	500,440.130	50	−45	−22	0.6027
5, 4, 1–5, 3, 2	1–1		500,947.302	50	23	19	
5, 4, 1–5, 3, 2	0–0		501,521.574	50	−18	−22	
16, 8, 9–16, 7, 9	0–1		504,693.126	50	68	−11	
9, 5, 4–9, 4, 5	1–1		504,911.265	50	−30	−30	
9, 5, 4–9, 4, 5	0–0		505,315.377	50	−38	−11	
8, 5, 4–8, 4, 4	0–1		507,611.451	50	−71	−54	
16, 8, 9–16, 7, 9	1–0		508,639.198	50	5	−66	
10, 5, 5–10, 4, 6	1–1		512,599.097	50	61	45	
10, 5, 5–10, 4, 6	0–0		512,873.710	50	−32	31	
4, 3, 1–4, 2, 3	0–1		513,087.953	50	−39	−31	
8, 5, 4–8, 4, 4	1–0		515,037.102	50	−49	−43	
4, 3, 1–4, 2, 3	1–0		522,355.415	50	−46	−53	
4, 2, 3–4, 1, 4	1–1	3–4	522,421.552	50	−15	26	0.0486
4, 2, 3–4, 1, 4	1–1	4–4	522,421.552	50	−15	26	0.9025
4, 2, 3–4, 1, 4	1–1	5–4	522,421.552	50	−15	26	0.0489
4, 2, 3–4, 1, 4	1–1	3–3	522,423.142	50	−22	21	0.3646
4, 2, 3–4, 1, 4	1–1	4–3	522,423.142	50	−22	21	0.0243
4, 2, 3–4, 1, 4	1–1	4–5	522,423.142	50	−22	21	0.0244
4, 2, 3–4, 1, 4	1–1	5–5	522,423.142	50	22	21	0.5867
4, 2, 3–4, 1, 4	0–0	4–4	522,736.348	50	−52	−23	
4, 2, 3–4, 1, 4	0–0	3–3	522,737.946	50	16	46	0.3833
4, 2, 3–4, 1, 4	0–0	5–5	522,737.946	50	16	46	0.6167
9, 4, 5–9, 3, 6	1–1		532,057.144	50	67	13	
9, 4, 5–9, 3, 6	0–0		532,209.162	50	52	78	
6, 2, 4–6, 1, 5	1–1		543,980.527	50	1	2	
6, 2, 4–6, 1, 5	0–0		544,179.908	50	−13	−63	
4, 4, 1–4, 3, 1	0–1		546,252.078	50	16	−7	
4, 1, 4–3, 2, 2	0–1	3–2	547,352.765	50	−11	−7	0.3573
4, 1, 4–3, 2, 2	0–1	3–3	547,352.765	50	−11	−7	0.0313
4, 1, 4–3, 2, 2	0–1	5–4	547,352.765	50	−11	−7	0.6114
4, 1, 4–3, 2, 2	0–1	4–3	547,354.709	50	−22	−15	0.9375
4, 1, 4–3, 2, 2	0–1	4–4	547,354.709	50	−22	−15	0.0625
4, 4, 1–4, 3, 1	1–0		555,367.932	50	5	−9	
3, 0, 3–2, 1, 1	0–1	2–1	572,942.971	50	27	13	0.3005
3, 0, 3–2, 1, 1	0–1	2–2	572,942.971	50	27	13	0.0556
3, 0, 3–2, 1, 1	0–1	4–3	572,942.971	50	27	13	0.6439
3, 0, 3–2, 1, 1	0–1	3–2	572,945.240	50	76	63	0.8889
3, 0, 3–2, 1, 1	0–1	3–3	572,945.240	50	76	63	0.1111
4, 4, 0–4, 3, 2	0–1		579,220.706	100	54	41	
13, 7, 7–13, 6, 7	0–1		581,758.233	50	−47	−60	
3, 0, 3–2, 1, 1	1–0	2–1	583,063.107	50	−68	−92	0.3005
3, 0, 3–2, 1, 1	1–0	2–2	583,063.107	50	−68	−92	0.0556
3, 0, 3–2, 1, 1	1–0	4–3	583,063.107	50	−68	−92	0.6439
3, 0, 3–2, 1, 1	1–0	3–3	583,065.375	50	−20	−42	0.1111
3, 0, 3–2, 1, 1	1–0	3–2	583,065.375	50	−20	−42	0.8889
13, 7, 7–13, 6, 7	1–0		586,906.553	50	26	11	
4, 4, 0–4, 3, 2	1–0		588,325.254	50	47	36	
12, 6, 6–12, 5, 7	1–1		593,242.326	50	109	151	

(*continued on next page*)

Table 3 (*continued*)

J'', K_a'', K_c''–J', K_a', K_c'	v''–v'	F''–F'	Freq.	Unc.	O–C 1	O–C 2	IW
12, 6, 6–12, 5, 7	0–0		593,562.750	50	−50	17	
5, 4, 2–5, 3, 3	1–1		594,588.376	50	17	19	
7, 5, 3–7, 4, 3	0–1		617,060.188	50	−47	−29	
7, 5, 3–7, 4, 3	1–0		624,470.175	50	−46	−41	
4, 2, 3–3, 3, 0	0–0		627,692.811	50	39	70	
4, 2, 3–3, 3, 1	1–0		636,409.635	50	−35	−18	
6, 3, 4–6, 2, 5	0–0		654,683.364	50	12	−9	
5, 3, 2–5, 2, 4	1–0		664,390.498	50	−32	−46	
6, 4, 2–6, 3, 4	0–1		665,161.928	50	17	7	
3, 1, 2–2, 2, 0	1–0		672,369.984	50	−87	−70	
6, 4, 2–6, 3, 4	1–0		673,580.494	50	−19	−46	
8, 2, 6–7, 5, 2	1–0		683,365.874	30	−61	−11	
6, 5, 1–6, 4, 2	0–0		694,067.161	50	−51	−51	
6, 5, 2–6, 4, 2	1–0		696,885.061	50	7	−5	
15, 8, 8–15, 7, 8	0–1		698,630.395	20	−20	−8	
2, 1, 1–1, 0, 1	0–1		699,224.180	50	−80	−64	
15, 8, 8–15, 7, 8	1–0		702,712.022	20	−6	−21	
2, 1, 1–1, 0, 1	1–0		709,349.894	50	−116	−106	
15, 7, 8–15, 6, 9	1–1		723,705.986	20	2	−6	
5, 5, 1–5, 4, 1	0–1		723,770.389	20	−20	−37	
15, 7, 8–15, 6, 9	0–0		723,893.601	20	−5	−44	
5, 5, 0–5, 4, 1	0–0		727,837.183	20	17	8	
5, 5, 0–5, 4, 1	1–1		728,315.873	20	−16	−17	
6, 5, 1–6, 4, 3	0–1		730,963.745	20	16	15	
5, 5, 1–5, 4, 1	1–0		732,022.787	20	−32	−22	
6, 5, 2–6, 4, 3	0–0		733,183.042	20	−64	−69	
5, 5, 0–5, 4, 2	0–1		733,675.812	20	22	−1	
6, 5, 2–6, 4, 3	1–1		733,781.575	20	4	−9	
5, 5, 1–5, 4, 2	0–0		737,375.281	20	13	3	
5, 5, 1–5, 4, 2	1–1		737,861.429	20	−14	−18	
7, 5, 3–7, 4, 4	1–1		738,581.147	20	−17	−15	
7, 5, 3–7, 4, 4	0–0		739,145.522	20	−14	−22	
6, 5, 1–6, 4, 3	1–0		739,529.798	20	45	32	
5, 0, 5–4, 1, 3	0–1		739,540.800	40	−24	−42	
5, 5, 0–5, 4, 2	1–0		741,920.745	20	−3	2	
9, 3, 6−8, 6, 2	0–1		746,536.091	20	−7	−40	
9, 6, 4–9, 5, 4	0–1		747,808.211	20	28	48	
7, 5, 2–7, 4, 4	0–1		748,035.832	20	−8	−12	
12, 7, 6–12, 6, 6	0–1		748,141.329	20	12	−10	
12, 7, 6–12, 6, 6	1–0		753,365.354	20	−4	−12	
9, 6, 4–9, 5, 4	1–0		754,142.246	20	−3	−18	
12, 5, 7–12, 4, 8	1–1		754,871.209	20	9	33	
9, 3, 6–8, 6, 2	1–0		755,371.685	20	12	7	
7, 5, 2–7, 4, 4	1–0		755,400.481	20	−5	−15	
8, 5, 4–8, 4, 5	1–1		764,073.310	20	−44	−44	
8, 5, 4–8, 4, 5	0–0		764,549.386	20	−16	−25	
6, 1, 6–5, 2, 4	0–1		764,615.925	100	53	64	
9, 6, 3–9, 5, 4	1–1		765,572.975	20	−77	−37	
9, 6, 3–9, 5, 4	0–0		766,222.250	20	−34	−56	

3, 1, 3,–2, 0, 2	1–1	769,244.730	20	17	4
3, 1, 3,–2, 0, 2	0–0	769,268.979	50	9	14
9, 2, 7–8, 5, 3	0–1	773,844.975	200	−76	−24
6, 1, 6–5, 2, 4	1–0	774,626.648	100	14	−12
7, 3, 5–7, 2, 6	0–0	774,633.321	100	14	−39
6, 2, 5–6, 1, 6	0–0	787,458.383	50	−5	40
2, 2, 0–1, 1, 0	0–1	795,582.067	50	−38	−22
2, 2, 0–1, 1, 0	1–0	805,425.192	50	−71	−76
8, 5, 3,–8, 4, 5	0–1	807,083.150	50	−4	4
7, 4, 3–7, 3, 5	1–0	811,790.309	50	−1	−55
4, 2, 2–3, 3, 0	0–1	815,531.668	50	−59	−49
16, 7, 9–16, 6, 10	1–1	856,171.217	400	−677	−553
16, 7, 9–16, 6, 10	0–0	856,220.960	40	5	26
18, 9, 9–18, 8, 10	1–1	858,226.129	100	5	46
18, 9, 9–18, 8, 10	0–0	858,660.416	100	40	188
7, 1, 7–6, 2, 5	1–0	860,804.814	40	−20	−42
7, 0, 7–6, 1, 5	0–1	863,214.082	40	−48	−56
3, 3, 1–3, 0, 3	0–1	866,371.263	40	23	47
7, 6, 2–7, 5, 2	0–1	870,382.696	20	−27	−4
7, 0, 7–6, 1, 5	1–0	873,321.458	20	10	1
7, 6, 1–7, 5, 2	0–0	874,159.210	20	27	25
7, 6, 1–7, 5, 2	1–1	874,804.743	50	51	46
3, 3, 0–3, 0, 3	1–1	876,120.388	50	11	40
8, 6, 2–8, 5, 4	0–1	876,351.627	20	37	22
14, 8, 7–14, 7, 7	0–1	876,399.669	30	25	48
9, 6, 4–9, 5, 5	1–1	877,108.694	30	−2	16
3, 3, 1–3, 0, 3	1–0	877,314.918	50	12	23
9, 6, 4–9, 5, 5	0–0	877,684.034	30	65	91
8, 6, 3–8, 5, 4	0–0	877,781.005	50	−11	20
7, 6, 2–7, 5, 2	1–0	877,841.488	30	21	32
6, 3, 3–6, 2, 5	0–1	878,958.147	50	−16	−59
8, 6, 3–8, 5, 4	1–1	879,116.879	30	39	46
12, 5, 7–11, 8, 3	0–1	879,460.798	50	−50	37
11, 7, 5–11, 6, 5	0–1	879,979.707	50	187	168
14, 8, 7–14, 7, 7	1–0	880,520.805	20	−7	19
7, 6, 1–7, 5, 3	0–1	883,613.886	20	26	19
11, 4, 7–11, 3, 8	1–1	884,216.355	30	−32	6
11, 4, 7–11, 3, 8	0–0	884,404.908	30	18	42
8, 6, 2–8, 5, 4	1–0	884,568.080	30	77	66
8, 2, 6–8, 1, 7	1–1	884,613.291	20	7	−8
8, 2, 6–8, 1, 7	0–0	885,011.431	70	−22	−124
11, 7, 5–11, 6, 5	1–0	885,181.009	20	15	10
12, 5, 7–11, 8, 3	1–0	886,133.711	30	7	−23
7, 6, 2–7, 5, 3	0–0	886,637.661	10	12	8
7, 6, 2–7, 5, 3	1–1	887,296.139	20	−4	1
6, 3, 3–6, 2, 5	1–0	888,161.714	30	−6	−45
9, 6, 3–9, 5, 5	0–1	889,188.719	20	−12	−1
10, 2, 8–9, 5, 5	0–0	890,071.601	40	47	110
6, 6, 1–6, 5, 1	0–1	890,753.398	20	−14	21
10, 2, 8–9, 5, 5	1–1	890,914.033	100	−3	−84
3, 1, 2–2, 0, 2	0–1	1,047,378.479	50	30	51

(*continued on next page*)

Table 3 (*continued*)

J'', K_a'', K_c''–J', K_a', K_c'	v''–v'	F''–F'	Freq.	Unc.	O–C 1	O–C 2	IW
3, 1, 2–2, 0, 2	1–0		1,057,461.679	50	69	100	
3, 2, 1–2, 1, 1	0–1		1,081,970.535	100	21	28	
12, 8, 4–12, 7, 5	0–0		1,106,168.099	100	25	−51	
12, 8, 5–12, 7, 5	1–0		1,109,998.339	100	57	121	
7, 2, 6–6, 3, 4	0–1		1,127,032.109	100	16	95	
7, 2, 6–6, 3, 4	1–0		1,136,215.519	100	45	81	
3, 2, 2,–2, 1, 2	0–1		1,145,320.392	200	70	114	
12, 8, 5–12, 7, 6	1–1		1,157,447.781	100	−74	−67	
13, 8, 5–13, 7, 7	0–1		1,157,465.155	100	−290	−310	
5, 2, 3–4, 3, 1	1–0		1,157,582.587	200	−36	7	
11, 8, 4–11, 7, 4	1–0		1,158,907.728	200	241	250	
10, 5, 5–10, 4, 7	1–0		1,167,978.523	300	202	194	
11, 8, 3–11, 7, 5	0–1		1,169,771.899	100	−111	−306	
7, 3, 4–7, 2, 6	0–1		1,170,701.479	200	113	34	
11, 8, 3–11, 7, 5	1–0		1,175,425.821	100	−106	−167	
10, 8, 2–10, 7, 4	0–1		1,183,885.875	100	−78	−280	
5, 2, 3–4, 3, 2	1–1		1,185,110.993	100	−78	−31	
10, 8, 3–10, 7, 4	1–1		1,187,141.250	100	−22	−71	
10, 8, 2–10, 7, 3	0–0		1,187,149.499	100	−35	−151	
13, 7, 6–13, 6, 8	1–0		1,187,405.893	100	26	209	
10, 8, 3–10, 7, 3	1–0		1,190,404.852	100	−1	37	
10, 2, 8–10, 1, 9	0–0		1,191,348.579	100	123	95	
5, 0, 5–4, 1, 4	0–0		1,192,696.884	100	−60	−42	
14, 8, 6–14, 7, 8	0–1		1,193,114.886	500	−511	−585	
7, 3, 5–6, 4, 2	0–0		1,236,503.548	200	60	95	
4, 3, 2–3, 2, 2	0–1		1,556,001.308	100	76	106	
4, 3, 2–3, 2, 2	1–0		1,565,266.523	100	−41	−34	
6, 2, 5–5, 1, 4	1–1		1,590,323.445	100	23	41	
4, 3, 1–3, 2, 2	0–0		1,592,795.008	100	−4	6	
7, 2, 5−6, 3, 3	1–0		1,621,154.874	100	38	116	
7, 3, 4–6, 4, 2	0–1		1,633,336.458	300	132	115	
7, 3, 4–6, 4, 2	1–0		1,641,690.737	100	13	21	
7, 0, 7–6, 1, 6	0–0		1,642,871.129	100	−7	24	
7, 0, 7–6, 1, 6	1–1		1,642,947.145	100	87	131	
7, 1, 7–6, 0, 6	0–0		1,643,328.613	100	17	49	
7, 1, 7–6, 0, 6	1–1		1,643,403.049	100	105	147	
5, 3, 3–4, 2, 2	0–0		1,683,711.264	200	36	77	
4, 4, 0–3, 3, 0	0–1		1,691,440.688	100	−42	−38	
4, 4, 1–3, 3, 1	0–1		1,694,381.370	100	−51	−49	
4, 4, 0–3, 3, 1	1–1		1,700,009.486	100	−2	14	
4, 4, 0–3, 3, 0	1–0		1,701,928.417	200	55	70	
8, 4, 4–7, 5, 2	0–1		1,732,662.471	100	84	75	
6, 5, 1–5, 4, 1	0–1		2,409,847.645	200	252	269	
6, 5, 2–5, 4, 2	0–1		2,417,810.376	200	431	441	
7, 3, 4–6, 2, 4	0–1		2,425,421.623	200	575	516	
7, 2, 6–6, 1, 6	1–0		2,578,357.087	200	−126	−67	

For overlapping lines, the residuals refer to the intensity weighted average. In these instances, the intensity weights IW are given.

Table 4
Spectroscopic parameters[a] (MHz) for the ground state of ND_2H

	Fit 1[b]		Fit 2	
F	3129.951(101)		3129.586(106)	
F_K	−9.327(34)		−9.114(36)	
F_J	0.8529(40)		0.8335(45)	
F_{KK}	0.02401(85)		0.01331(95)	
$F_{JK}\times10^3$	0.383(290)		2.814(228)	
$F_{JJ}\times10^3$	−1.521(35)		−1.5143(235)	
$F_{KKK}\times10^3$	0.03216(195)			
$F_{JKK}\times10^3$	−0.02250(102)			
$F_{JJK}\times10^6$	−3.090(84)			
$F_{JJJ}\times10^6$	−0.0949(105)		−0.848(65)	
	Parameter[c]	Difference[d]	Parameter[c]	Difference[d]
E	0[e]	5118.8906(105)	0[e]	5118.9055(101)
A	223,187.69675(268)	16.11937(158)	223,187.70141(265)	16.12050(158)
B	160,214.9878(98)	5.32771(85)	160,215.0026(108)	5.33140(81)
C	112,520.7649(105)	−4.08516(61)	112,520.7453(112)	−4.08672(74)
D_K	19.28764(135)	0.043865(146)	19.28318(129)	0.043664(128)
D_{JK}	−2.94660(168)	0.010052(62)	−2.94014(164)	0.010293(53)
$D_J\times10^3$	3,520.349(288)	0.9329(87)	3,519.173(284)	0.9139(78)
$d_1\times10^3$	−1,234.235(265)	−0.7764(43)	−1,233.023(294)	−0.8036(61)
$d_2\times10^3$	−279.277(145)	−1.77392(243)	−279.902(142)	−1.78665(248)
$H_K\times10^3$	5.631(55)	0.0506(35)	4.946(60)	0.0538(35)
$H_{KJ}\times10^3$	0.731(84)	0.06719(197)	1.776(89)	0.06099(234)
$H_{JK}\times10^6$	−660.0(320)	−0.57(52)	−1043.8(312)	3.85(41)
$H_J\times10^6$	306.13(250)	−1.055(58)	323.38(181)	−1.497(54)
$h_1\times10^6$	254.51(244)	0.4716(192)	248.76(186)	0.644(35)
$h_2\times10^6$	54.66(131)	1.3860(237)	45.33(97)	1.5961(243)
$h_3\times10^6$	15.32(43)	1.0749(159)	20.65(49)	0.9739(119)
$L_K\times10^6$	−2.887(47)	0.2099(194)	−3.550(157)	0.1015(167)
$L_{KKJ}\times10^6$	0.490(45)	−0.3879(271)	2.136(241)	−0.2156(121)
$L_{JK}\times10^6$		0.0731(102)	−0.953(97)	
$L_{JJK}\times10^6$			−0.0554(114)	
$L_J\times10^9$	−47.59(178)	1.996 (124)		3.534(110)
$l_1\times10^9$			55.0(51)	−0.489(62)
$l_2\times10^9$		−1.263(56)	−19.34(130)	−2.002(52)
$l_3\times10^9$		−0.592(73)	−5.37(49)	
$l_4\times10^9$	−1.788(110)	−0.4490(310)	−1.257(158)	−0.5488(284)
χ_{cc}	−3.8667(145)		−3.8627(145)	
χ_{bb}	1.8186(121)		1.8212(120)	

[a] F is an abbreviation for F_{bc}; see also Section 5. Numbers in parentheses are one standard deviation in units of the least significant figures.
[b] Prefered fit.
[c] $X=(X_0+X_1)/2$.
[d] $\Delta X=(X_0-X_1)/2$.
[e] Per definitionem.

c-component of the dipole moment is considerably larger than the b-component. Transition frequencies were predicted using $\mu_c=1.47$ D and $\mu_b=0.21$ D, values derived from $\mu=1.486$ D and $\theta_R=-8.12°$. Analogous calculations for NH_2D were in agreement with dipole moment components determined by Stark effect measurements [6].

As already discussed in Ref. [6], the sign of F cannot be determined in the fit. Nevertheless, the sign of the product of F, μ_b, and μ_c affects strongly the intensities of several transitions involving perturbed levels. As is shown in Fig. 5, considering the transition $J_{K_aK_c}=7_{3,5}$–$7_{2,6}$, $v=0$–0 as an example, F had to be positive, when both μ_b and μ_c were chosen to be positive. The simulation with final fit parameters, shown in the middle trace, reproduces the line profile of both transitions with comparable intensities quite well, whereas in the case of sign reversal of, e.g. μ_c, the simulation (lower trace) deviates obviously from the experimental spectrum (upper trace).

6. Discussion

The quality of the two fits obtained in the presented work is excellent as they describe the extensive and very diverse dataset of a complex spectrum within experimental uncertainties. The terms of eighth order are correlated. Therefore, the values of the respective parameters are strongly affected by the particular choice of the parameters as can be seen in Table 4 and should be interpreted with caution. Since centrifugal distortion effects are rather large in light hydride species such as ND_2H the choice of the highest order parameter affects the lower order parameters outside the model-dependent

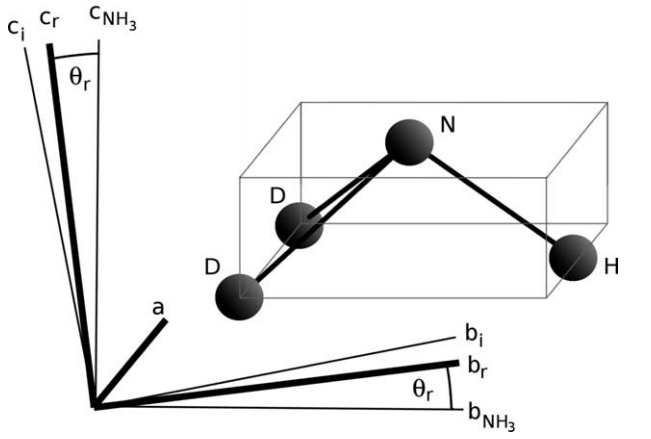

Fig. 4. Sketch of the position of the reduced axis system (r) and the inertial axis system (i) with respect to the NH_3 reference system in which c_{NH_3} is perpendicular to the plane spanned by the three hydrogen atoms. The *a*-axis coincides in all systems. The proper orientation of the ND_2H molecule is also shown (The molecule has been shifted for clarity; the origin of the coordinate systems is slightly below the N-atom).

uncertainties. In contrast to fit 1, fit 2 has a reduced set of Coriolis interactions terms which seems favorable. On the other hand, the transition frequencies obtained in the present study have been better reproduced in fit 1 in which the weighted standard deviation is 0.99 compared with 1.12 in fit 2. Therefore, fit 1 is viewed as the preferred one. The differences in fits 1 and 2 are expected to be negligible for the prediction of transition frequencies for astronomical observations.

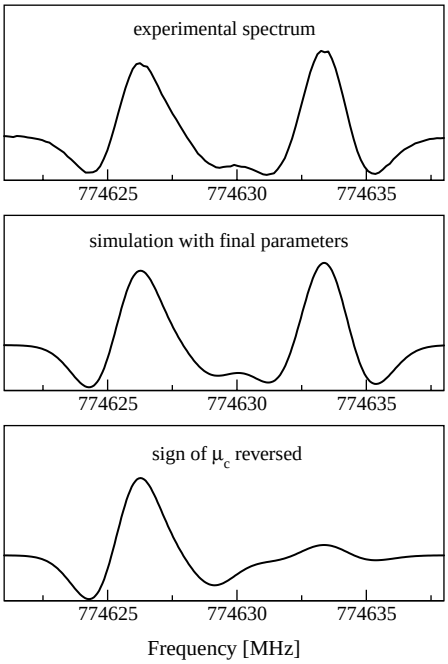

Fig. 5. The upper trace shows the $J_{K_a,K_c} = 6_{1,6}$–$5_{2,4}$, $v=0$–0 and $J_{K_a,K_c} = 7_{3,5}$–$7_{2,6}$, $v=0$–0 transitions towards lower and upper frequencies, respectively. The simulation with final fitting parameters, shown in the middle trace, reproduces the line profile of both, comparable intense transitions very well. In case of reversed sign of, e.g. μ_c, the simulation in the lower trace deviates obviously from the experimental spectrum.

Fit 1 and fit 2 are expected to converge to the same set of parameters if more accurate transitions frequencies are recorded. These transitions will involve even higher quantum numbers at still higher frequencies or with even lower intensities. Although, interesting from the spectroscopic point of view these transitions are irrelevant for astronomical observations because the energy levels involved are too high.

7. Conclusion

The present work demonstrates the first successful application of superlattice multipliers to record high-resolution molecular spectra far into the terahertz region. This technique permitted to extend the experimental dataset on ND_2H with kilohertz accuracy up to 2.6 THz. Energy levels accessed extend to $J=18$ and $K_a=9$ corresponding to an energy of more than 1800 cm^{-1}.

Greatly improved spectroscopic parameters have been obtained. In particular, the description of the Coriolis interaction between the two tunneling states has been refined substantially. Thus, transitions up to $J=15$ and $K_a=9$ should be found within 1 MHz of the predictions. Transitions involving low-lying rotational levels, which are most important for astronomical observations, are predicted to better than 100 kHz. The quantum number range and the accuracy of the predictions is sufficient for astronomical observations. These predictions will be made available in the Cologne database for molecular spectroscopy (www.cdms.de) [10].

Acknowledgements

We thank Frank W. Maiwald and Peter H. Siegel from the Jet Propulsion Laboratory, Pasadena, CA, for providing the 2.4 THz Schottky barrier tripler for some of the measurements. This work has been supported by the Deutsche Forschungsgemeinschaft (DFG) via grant SFB 494 and by the Ministry of Science and Technology of the Land Nordrhein-Westfalen.

Supplementary Material

Supplementary data associated with this article can be found, in the online version, at doi:10.1016/j.molstruc.2006.03.035. Supplementary material for this article is available on ScienceDirect (www.sciencedirect.com).

References

[1] M. Wiedner, G. Schmidt, F. Bielau, M. Emprechtinger, U.U. Graf, R. Güsten, C.E. Honingh, K. Jacobs, D. Rabanus, K. Rettenbacher, J. Stutzki, N. Volgenau, Astron. Astrophys, submitted for publication.
[2] E. Roueff, S. Tiné, L.H. Coudert, G. Pineau des Forêts, E. Falgarone, M. Gerin, Astron. Astrophys. 354 (2000) L63–L66.
[3] F.F.S. van der Tak, P. Schilke, H.S.P. Müller, D.C. Lis, T.G. Phillips, M. Gerin, E. Roueff, Astron. Astrophys. 388 (2002) L53–L56.
[4] D.C. Lis, E. Roueff, M. Gerin, T.G. Phillips, L.H. Coudert, F.F.S. van der Tak, P. Schilke, Astrophys. J. 571 (2002) L55–L58.
[5] F.C. De Lucia, P. Helminger, J. Mol. Spectrosc. 54 (1975) 200–214.

[6] E.A. Cohen, H.M. Pickett, J. Mol. Spectrosc. 93 (1982) 83–100.
[7] L. Fusina, D. Di, J.W.C. Johns, L. Halonen, J. Mol. Spectrosc. 127 (1988) 240–254.
[8] F. Maiwald, F. Lewen, V. Ahrens, M. Beaky, R. Gendriesch, A.N. Koroliev, A.A. Negirev, D.G. Paveljev, B. Vowinkel, G. Winnewisser, J. Mol. Spectrosc. 202 (2000) 166–168.
[9] C.P. Endres, F. Lewen, D.G. Paveliev, in preparation.
[10] H.S.P. Müller, F. Schlöder, J. Stutzki, G. Winnewisser, J. Mol. Struct. 742 (2005) 215–227.
[11] F. Lewen, R. Gendriesch, I. Pak, D.G. Paveliev, M. Hepp, R. Schieder, G. Winnewisser, Rev. Sci. Inst. 69 (1998) 32–39.
[12] M. Winnewisser, H. Lichau, F. Wolf, J. Mol. Spectrosc. 202 (2000) 155–162.
[13] D.G. Paveliev, I.Yu. Koschurinov, F. Lewen, C. Endres, V.M. Ustinov, A.M. Baryshev, A.E. Zhukov, Proceedings of the Joint 30th International Conference on Infrared and Millimeter Waves and 13th International Conference on Terahertz Electronics, September 19–23, vol. 1, Williamsburg, VA, USA, 2005, pp. 140–141.
[14] R. Scheuerer, D.G. Pavelev, K.F. Renk, E. Schomburg, Physica E 22 (2004) 797–803.
[15] B.J. Drouin, F.W. Maiwald, J.C. Pearson, Rev. Sci. Instrum. 76 (2005) 093113.
[16] S.P. Belov, Š. Urban, G. Winnewisser, J. Mol. Spectrosc. 189 (1998) 1–7.
[17] H.M. Pickett, J. Chem. Phys. 56 (1972) 1715–1723.
[18] H.M. Pickett, J. Mol. Spectrosc. 148 (1991) 371–377.
[19] Di G. Lonardo, A. Trombetti, Chem. Phys. Lett. 84 (1981) 327–330.
[20] M. Lichtenstein, J.J. Gallagher, V.E. Derr, J. Mol. Spectrosc. 12 (1964) 87–97.